

SUPPLEMENTARY INFORMATION

Quantum-assisted diamagnetic deflection of molecules

Yaakov Y. Fein^a, Armin Shayeghi^a, Filip Kiałka^a, Philipp Geyer^a, Stefan Gerlich^a and Markus Arndt^{*a}

^a Faculty of Physics, University of Vienna, Vienna, Austria

* Corresponding author. Email address: markus.arndt@univie.ac.at

Susceptibility calculation details

Geometries are extracted from the ab initio molecular dynamics simulations every picosecond for 10 ps and the resulting susceptibility tensors and geometry snapshots are given in Tables S1 and S2. Values of the molar magnetic susceptibility components are given in cgs units of 10^{-6} cm³/mol, as these are units often used in the chemistry community. To convert from cgs molar susceptibility to the SI mass susceptibility as used in the main text, multiply by $4\pi \times 10^{-9}/M$, with M the molar mass. The small off-diagonal susceptibility components (on average less than 1% of the isotropic susceptibility) for the vibrationally excited geometries are due to the chosen basis being the principal inertia axes for the ground-state geometry.

Extended experimental details

Velocity measurements and gating. The velocity spectrum was obtained via direct time-of-flight triggered by the gas pulse trigger and collected with a fast counting card (FAST ComTec P7882). Given the length from the source to detector (3.77 m) one can directly calculate the velocity, taking into account a measured delay of about 25 μ s between the TTL trigger signal to the current pulse in the valve and an additional ~ 40 μ s delay between the current pulse and the beginning of the gas flow.¹ The time-of-flight is gated by a switch which is held open for a 1 ms window around the pulse arrival time, as shown in Figure S1.

Data analysis and extended discussion

Drift correction. The individual interference curves are fitted to sines with a robust (bi-square) least squares fit. The weighted mean of the differences of the phases provides an estimate of the deflection. In the case of adamantane, the phase of the reference data as a function of time is least square fitted to a first order polynomial, allowing the drift rate to be extracted. We then correct the data for this linear drift as shown in Figure S2 and extract the mean deflection in the same way as for anthracene (weighted mean of the phase differences).

Rotation and anisotropy in matter-wave interferometry. The effect of molecular rotation in matter-wave interferometers has been theoretically investigated in the framework of a Kapitza-Dirac Talbot-Lau interferometer,² which is similar to the scheme used here but with the second grating replaced by an optical phase grating. These results indicate a small modification to the visibility of the interference pattern as a function of Talbot length for a prolate top molecule. The visibility function enters as a weighting factor in the velocity averaging, but is typically a small correction on the order of a few percent, and so the non-rotating visibility function is used here.³

The use of anisotropic molecules in our setup also means that the effective open fraction of the material gratings is dependent on the molecular orientation. However, the difference is expected to be only on the order of a few percent, since polarizability enters only to the $1/6$ power in the calculation of the effective open fraction.³

Table S1 Anthracene molar susceptibility values in cgs units of $10^{-6} \text{ cm}^3/\text{mol}$ for the ground-state and 10 vibrationally excited geometries.

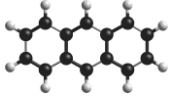
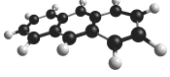
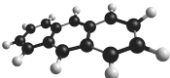
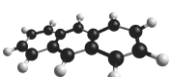
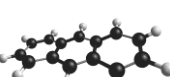
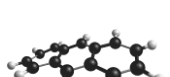
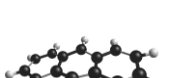
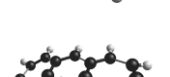
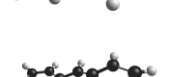
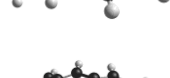
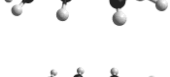
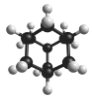
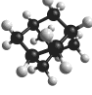
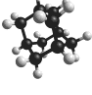
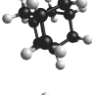
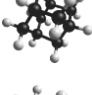
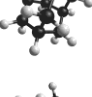
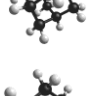
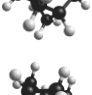
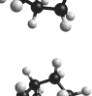
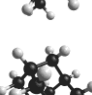
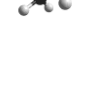
	χ_{mol}	Geometry
Ground-state geometry	$\begin{pmatrix} -73.4548 & 0.0010 & 0.0002 \\ 0.0010 & -263.6555 & 0.0001 \\ 0.0002 & 0.0001 & -65.2352 \end{pmatrix}$	
Geometry 1	$\begin{pmatrix} -72.3963 & 0.5353 & 0.9148 \\ 0.5353 & -259.1336 & 1.0876 \\ 0.9148 & 1.0876 & -66.5513 \end{pmatrix}$	
Geometry 2	$\begin{pmatrix} -69.3955 & 0.6519 & -1.7581 \\ 0.6519 & -255.2110 & -1.4503 \\ -1.7581 & -1.4503 & -69.7971 \end{pmatrix}$	
Geometry 3	$\begin{pmatrix} -70.9703 & 1.6777 & -2.1776 \\ 1.6777 & -259.5842 & 1.8797 \\ -2.1776 & 1.8797 & -66.6521 \end{pmatrix}$	
Geometry 4	$\begin{pmatrix} -73.3642 & -0.2194 & 0.1982 \\ -0.2194 & -264.4239 & -0.5727 \\ 0.1982 & -0.5727 & -66.4374 \end{pmatrix}$	
Geometry 5	$\begin{pmatrix} -76.6015 & 1.2071 & -3.0094 \\ 1.2071 & -252.0890 & 2.4380 \\ -3.0094 & 2.4380 & -64.1553 \end{pmatrix}$	
Geometry 6	$\begin{pmatrix} -71.5495 & -0.6913 & 0.0875 \\ -0.6913 & -265.4529 & 0.3772 \\ 0.0875 & 0.3772 & -66.2484 \end{pmatrix}$	
Geometry 7	$\begin{pmatrix} -73.6370 & -0.4398 & 0.3997 \\ -0.4398 & -260.9040 & 0.1279 \\ 0.3997 & 0.1279 & -67.2955 \end{pmatrix}$	
Geometry 8	$\begin{pmatrix} -74.1966 & 3.6559 & 0.5847 \\ 3.6559 & -256.3424 & 2.0224 \\ 0.5847 & 2.0224 & -64.3342 \end{pmatrix}$	
Geometry 9	$\begin{pmatrix} -77.1548 & 1.1671 & 1.4044 \\ 1.1671 & -256.3627 & 1.6444 \\ 1.4044 & 1.6444 & -63.5261 \end{pmatrix}$	
Geometry 10	$\begin{pmatrix} -70.2338 & -2.2486 & 1.7288 \\ -2.2486 & -261.2032 & -0.7479 \\ 1.7288 & -0.7479 & -68.7175 \end{pmatrix}$	

Table S2 Adamantane molar susceptibility values in cgs units of 10^{-6} cm³/mol for the ground-state and 10 vibrationally excited geometries.

	χ_{mol}	Geometry
Ground-state geometry	$\begin{pmatrix} -96.8763 & -0.0003 & 0.0004 \\ -0.0003 & -96.8819 & 0.0011 \\ 0.0004 & 0.0011 & -96.8833 \end{pmatrix}$	
Geometry 1	$\begin{pmatrix} -96.0826 & 0.5070 & 0.2194 \\ 0.5070 & -97.8343 & -0.4141 \\ 0.2194 & -0.4141 & -96.5287 \end{pmatrix}$	
Geometry 2	$\begin{pmatrix} -95.8598 & -0.3256 & 0.2201 \\ -0.3256 & -96.8969 & -0.1190 \\ 0.2201 & -0.1190 & -95.0229 \end{pmatrix}$	
Geometry 3	$\begin{pmatrix} -95.2936 & 0.0833 & -0.6679 \\ 0.0833 & -96.4373 & 0.1406 \\ -0.6679 & 0.1406 & -95.9999 \end{pmatrix}$	
Geometry 4	$\begin{pmatrix} -94.3205 & -0.3929 & 0.2529 \\ -0.3929 & -95.6332 & 0.2181 \\ 0.2529 & 0.2181 & -95.4062 \end{pmatrix}$	
Geometry 5	$\begin{pmatrix} -95.4311 & 0.1416 & 0.1933 \\ 0.1416 & -98.1770 & 0.0222 \\ 0.1933 & 0.0222 & -95.6698 \end{pmatrix}$	
Geometry 6	$\begin{pmatrix} -94.6069 & -0.6070 & 0.8700 \\ -0.6070 & -98.2014 & 0.2030 \\ 0.8700 & 0.2030 & -95.8140 \end{pmatrix}$	
Geometry 7	$\begin{pmatrix} -96.4424 & 0.2380 & 0.6144 \\ 0.2380 & -95.5733 & 0.0350 \\ 0.6144 & 0.0350 & -93.7945 \end{pmatrix}$	
Geometry 8	$\begin{pmatrix} -94.5478 & 0.9791 & -0.8995 \\ 0.9791 & -96.6673 & 0.1783 \\ -0.8995 & 0.1783 & -94.7064 \end{pmatrix}$	
Geometry 9	$\begin{pmatrix} -96.8547 & -0.9752 & 0.3240 \\ -0.9752 & -96.0442 & 1.1842 \\ 0.3240 & 1.1842 & -97.3175 \end{pmatrix}$	
Geometry 10	$\begin{pmatrix} -96.3551 & 0.0584 & 0.0971 \\ 0.0584 & -97.3500 & 0.4574 \\ 0.0971 & 0.4574 & -96.6491 \end{pmatrix}$	

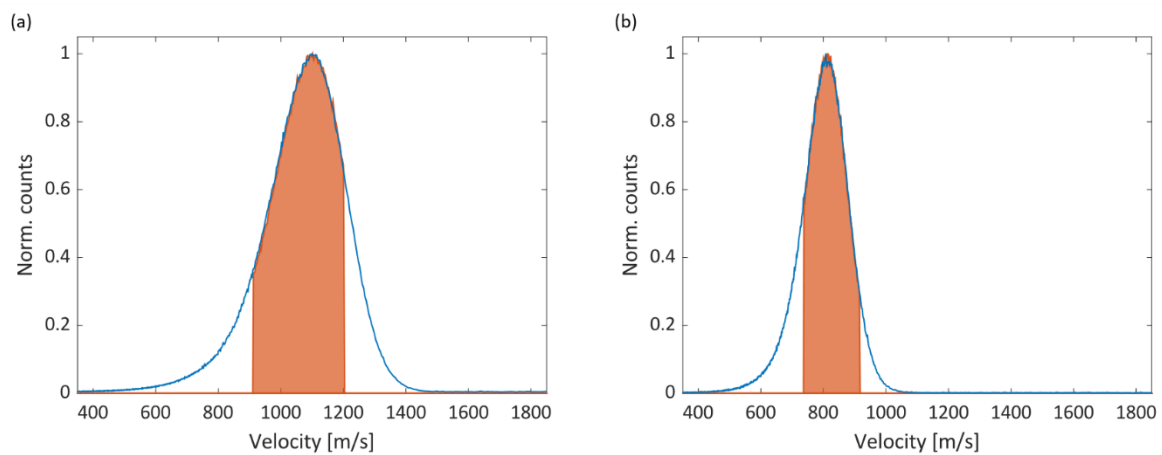


Figure S1 (a) Velocity spectra of anthracene, with the un gated signal shown in blue and the gated signal filled in red. (b) as in (a), for adamantane. The beam is slower in part due to the use of neon rather than helium as the seed gas.

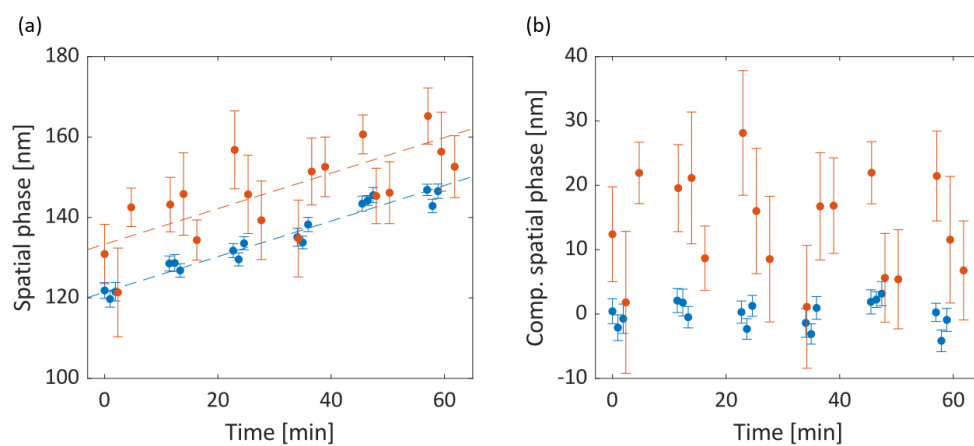


Figure S2 (a) Uncorrected phase data of adamantane as a function of the data-collection time, showing the reference data in blue and deflection data in red, with dashed lines linear fits. The slope for the deflection data is fixed as the fitted slope of the reference data. (b) Drift-compensated data, plotted relative to the reference data phase, as used in the calculation of the mean deflection.

Supplementary references

1. U. Even, *Advances in Chemistry*, 2014, **2014**, 1-11.
2. B. A. Stickler and K. Hornberger, *Phys. Rev. A*, 2015, **92**.
3. S. Nimmrichter and K. Hornberger, *Phys. Rev. A*, 2008, **78**, 023612.